NANO LETTERS

LETTER

pubs.acs.org/NanoLett

Growth, Defect Formation, and Morphology Control of Germanium–Silicon Semiconductor Nanowire Heterostructures

Shadi A. Dayeh,*[,†] Jian Wang,[‡] Nan Li,[†] Jian Yu Huang,[§] Aaron V. Gin,[§] and S. Thomas Picraux[†]

[†]Center for Integrated Nanotechnologies, Los Alamos National Laboratory, Los Alamos, New Mexico, United States

[‡]Materials Science and Technology Division, MST-8, Los Alamos National Laboratory, Los Alamos, New Mexico, United States

[§]Center for Integrated Nanotechnologies, Sandia National Laboratories, Albuquerque, New Mexico, United States

Supporting Information

ABSTRACT: By the virtue of the nature of the vapor–liquid–solid (VLS) growth process in semiconductor nanowires (NWs) and their small size, the nucleation, propagation, and termination of stacking defects in NWs are dramatically different from that in thin films. We demonstrate germanium–silicon axial NW heterostructure growth by the VLS method with 100% composition modulation and use these structures as a platform to understand how defects in stacking sequence force the ledge nucleation site to be moved along or pinned at a single point on the triple-phase circumference, which in turn determines the NW morphology. Combining structural analysis and atomistic simulation of the nucleation and propagation of stacking defects, we explain these observations based on preferred nucleation sites during NW growth. The stacking defects are found to provide a fingerprint of the layer-by-layer growth process and reveal how the 19.5° kinking in semiconductor NWs observed at high Si growth rates results from a stacking-induced twin boundary formation at the NW edge. This study provides basic foundations for an atomic level understanding of crystalline and defective ledge nucleation and propagation during [111] oriented NW growth and improves understanding for control of fault nucleation and kinking in NWs.

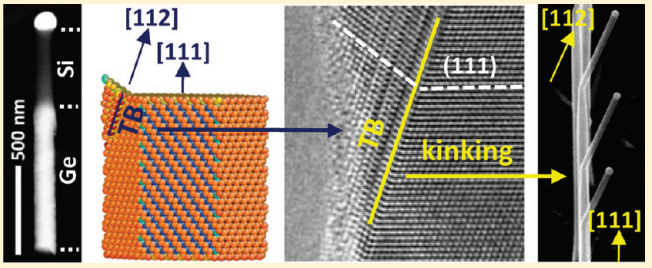

KEYWORDS: Nanowire, silicon, germanium, heterostructure, twin, kinking

Atomic level understanding of the growth processes that combine different materials enables a growth-by-design approach to implement device architectures for enhanced control over charge transport in semiconductors.[1] The vapor–liquid–solid (VLS) growth of nanowires (NWs) provides one route to achieve such heterostructures with the special advantage of being able to vary both doping and composition along the length of the NW, thereby enabling energy band-edge engineering in the charge transport direction.[2,3] Such band engineering along the length of the NW provides an added degree of freedom to tailor transport characteristics of transistors based on NW channel design, but has been challenging to accomplish in Ge–Si heterostructured NWs due to difficulties in rapid growth of high quality structures with large compositional changes. For VLS growth, these difficulties arise from the disparate growth temperatures and chemical potential-induced instabilities in the liquid growth seed upon switching between Si and Ge, which lead to interruption of growth, defect formation, and NW kinking. However, if controlled, these effects at heterostructure interfaces may be used as a fingerprint for investigating defect nucleation and propagation mechanisms during layer-by-layer growth in VLS grown NWs, providing new insight into the atomistics of NW growth. Prior work on NW growth defects and interfaces has emphasized III–V materials which generally exhibit stacking faults and polymorphs oriented perpendicular to the growth axis.[4−6] In a few other cases, twin boundaries parallel to the growth axis of Si NWs have been observed,[7,8] but the detailed mechanism by which they form and their relation to NW kinking[9,10] has not been previously reported.

Here, we exploit understanding of growth kinetics to achieve 100% axial composition modulation of Ge–Si NW heterostructures with liquid phase growth and utilize such heterostructures for tracking ledge nucleation of stacking defects and their propagation during their VLS growth. Precise sequencing of the gas precursor pressure and temperature upon transitioning from Ge to Si during VLS growth is shown to give pure Ge and pure Si NW segments with dimensions suitable for detailed structural study as well as for device applications. For typical Si segment growth rates (~8 nm/s) with high nucleation efficiency, we observe the onset of single two-dimensional defects near the heterostructure interface in the Si segment which propagates along the growing NW. These structures allow us to demonstrate key aspects of the VLS layer-by-layer growth mechanism, as well as advance current understanding for limiting defect and kink formation. This is accomplished through microscopy analysis and molecular dynamics (MD) simulations that strongly

Received: June 24, 2011
Revised: August 12, 2011
Published: August 30, 2011

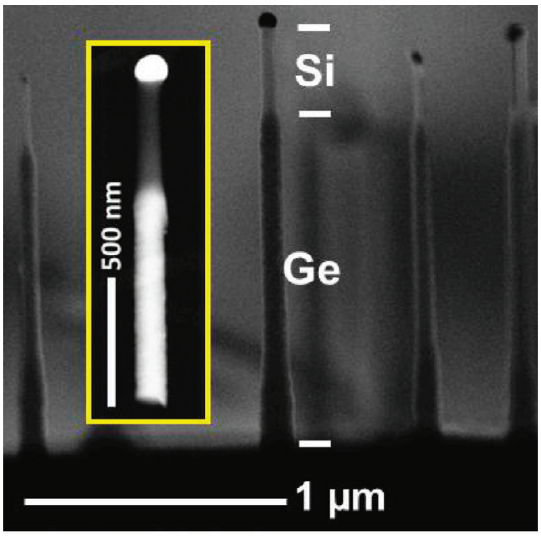

Figure 1. Cross-sectional SEM image of epitaxial Ge−Si heterostructure NWs on a Ge (111) substrate. The inset shows a *z*-contrast SEM image of a 100 nm diameter Ge−Si axial heterostructure with the Au growth seed at its tip.

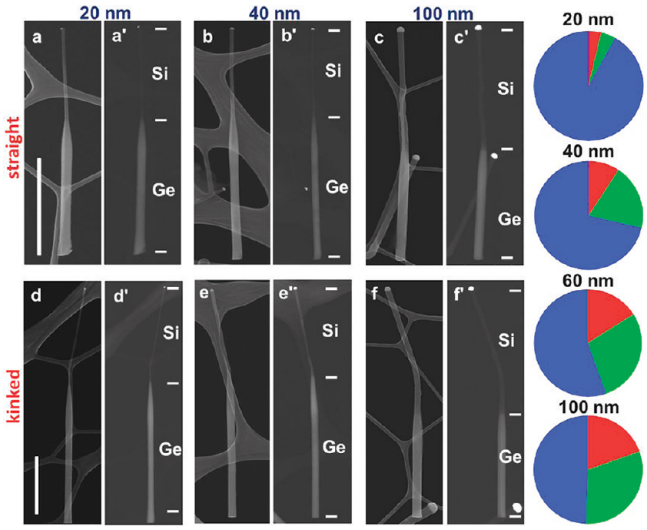

Figure 2. (a−c) SEM images of straight Ge−Si axial NW heterostructures with different starting Au colloid diameters, all synthesized simultaneously in the same growth run, and (a′−c′) their correspondent backscattering images showing distinct Ge and Si segments. (d−f) Typical Ge−Si axial NW heterostructures that display a systematic kink in the Si segment for any given diameter and (d′−f′) their correspondent backscattering images. The right panel shows statistical counts from wires grown on Ge(111) substrate (∼100 data points per diameter) accounting for different kink orientations with red (straight, [111] → [111]), green (kinked, [111] → ⟨112⟩), and blue (kinked, [111] → other ⟨111⟩). These SEM images are taken on TEM grids such that elemental mapping and analysis are not affected by the growth substrate. Scale bar in (a) for (a−c′) and in (d) for (d−f′) are 1 μm.

corroborate interpretation of the layer-by-layer growth process and provide the foundations for an atomic level understanding of crystalline and defective ledge nucleation and propagation in semiconductor NWs, without the requirement of in situ experiments. This understanding in turn provides insights for suppressing such defects and kinking in NWs.

One challenging obstacle for realizing 100% compositional modulation in germanium−silicon (Ge−Si) semiconductor NWs by VLS growth is the disparity in their growth temperatures due to differences in the precursor decomposition properties.[11,12] As a result, the reported composition modulation in VLS grown Si-SiGe heterostructure NWs has been typically limited to less than ∼30%.[13,14] Recently, abrupt Ge−Si heterostructure NWs with 100% composition modulation have been obtained using a solid Au−Al alloy catalyst for solid phase NW growth.[15] However, solid phase growth is much slower compared to its liquid phase counterpart, and the detailed growth mechanisms may not be the same as investigated here for liquid mediated growth.

Single phase VLS NW growth typically occurs at ∼270−380 °C for Ge using GeH_4 and 400−600 °C for Si using SiH_4.[16] For heterostructure NW growth, it has been observed that while switching from one material to another, the differences of surface energy[17,18] and chemical potential[19] between the Au alloy seed and the two materials may destabilize the Au particle and prevent layer-by-layer axial elongation. In that case, off-axis (kinked) growth or Au seed slippage from the top of the NW and growth down the NW sidewalls often occurs.[9,19] Such undesired growth has also been observed during synthesis of homogeneous NWs for growth at too low temperatures or high partial pressures.[9] We find that maintaining a liquid Au particle with high supersaturation is required to start the epitaxial growth of a Si segment on the previously grown Ge NW, as well as to stabilize the Au seed on top of the NW and prevent kinking. Such 100% Ge to Si growth is demonstrated in Figure 1 by pulsing GeH_4 (30% in H_2) after a temperature ramp from 270 to 440 °C, followed by immediate introduction of SiH_4 (50% in H_2) to carry out the Si segment growth. Here, the Ge NW nucleation was carried at ∼380 °C for 2 min followed by Ge NW elongation for 5 min at ∼270 °C both at 2 Torr chamber pressure (0.6 Torr GeH_4 partial pressure), after which the temperature was ramped to 440 °C with a ramp rate of 2 °C/s and was stabilized for 7 min prior to pulsing GeH_4 for 25 s (0.3 Torr GeH_4 partial pressure) followed by SiH_4 flow for 30 s at ∼3 Torr chamber pressure (1.5 Torr SiH_4 partial pressure) to grow the Si segment without any pump/purge in between the two gases. Without pulsing GeH_4 prior to SiH_4 flow, deficiency in nucleation and wormlike growth of the Si segment were observed with no well-defined long-range growth orientation. A second successful growth method is to maintain the GeH_4 precursor pressure during the temperature ramp and then switching to SiH_4 at the Si segment growth temperature (Figure 2). Here, the Ge NWs were nucleated at ∼370 °C for 1.5 min at 2 Torr followed by Ge NW elongation for 10 min at ∼270 °C, both at 2 Torr chamber pressure (0.6 Torr GeH_4 partial pressure), after which the temperature was ramped to ∼430 °C with a ramp rate of 2 °C/s in the presence of GeH_4 flow (0.5 Torr chamber pressure, 0.15 Torr GeH_4 partial pressure) at which GeH_4 was switched off and SiH_4 was switched on for 1.5 min at ∼2.8 Torr chamber pressure (1.4 Torr SiH_4 partial pressure) without any pump/purge in between the two gases. We note here that maintaining the GeH_4 partial pressure during temperature ramp leads to additional vapor−solid deposition of Ge on the Ge NW sidewalls resulting in a larger diameter Ge NW segment compared to that of the starting Au colloid and Si NW segment. Both methods result in high yield epitaxial growth of Ge−Si axial NW heterostructures with 100% composition modulation and without Si radial overcoating on the Ge segment. However, increasing the temperature in vacuum or H_2 ambient leads to Au diffusion on the NW sidewalls,[19] which was confirmed by transmission electron microscopy (TEM), and induces surface roughness

dx.doi.org/10.1021/nl202126q |*Nano Lett.* 2011, 11, 4200–4206

due to Au-catalyzed sidewall growth, as can be readily observed on the Ge segment in the scanning electron microscope (SEM) image inset of Figure 1. Keeping a GeH_4 overpressure during the temperature ramp maintains layer-by-layer growth throughout the temperature cycling and prevents Au diffusion; it also enhances the vapor−solid growth rate on the Ge-NW sidewalls that leads to a larger Ge NW diameter compared to the starting Au colloid diameter. Such heterostructured NWs have demonstrated several orders of magnitude superior device performance over their homogeneous counterparts as discussed elsewhere.[20] We focus here on atomic level analysis of the VLS growth process in terms of the nucleation of defects and the role of these defects in modulating the nanowire structure. We also noted that for the NWs shown in Figure 2, the SiGe transition region (composition change from 10 to 90%, Supporting Information Figure S1) was found to be $\sim 0.85d - 1.4d$ for $d = 40-100$ nm, where d is the NW diameter, and $\sim 2d$ for $d \leq 30$ nm due to enhanced solute concentrations at small diameters.[21] It is also possible that the presence of GeH_4 in the chamber when SiH_4 is introduced has also an effect on the length of the transition regions, however, such effect could not be isolated because pumping GeH_4 from the chamber prior to SiH_4 introduction leads to destabilization of the Au growth seed. Such transition regions ($\sim d$) are typical for liquid phase growth,[14] and while long compared to the abrupt transition observed for growth using a solid catalyst,[15] they allow the realization of novel bandgap engineered devices.[20]

In the VLS mechanism, growth is understood to proceed in a layer-by-layer process with ledge nucleation occurring at the triple-phase interface.[22,23] Thus nucleation and propagation of defects during growth in semiconductor NWs can be dramatically different from that observed in thin films where defects can nucleate at many sites such as grain boundary, surfaces, etc., whereas the nucleation of defects in NWs likely occurs at the edge of their faceted surface due to the small cross-section across their diameter. Particularly at higher supersaturations and growth rates in NWs, the probability of stacking adatoms at faulted locations is expected to be non-negligible. Such effects are relevant here to the Si segments of the heterostructure NWs where Si is known to have higher supersaturations in Au relative to Ge,[24] and generally tend to grow in ⟨211⟩ orientations at higher SiH_4 partial pressures[25] that favor enhanced nucleation efficiencies.

Detailed analysis of the microstructure of the Si segments of our Ge−Si heterostructures, as shown in Figure 3, reveals the presence of a single fault per NW segment that nucleates from the same NW facet (left side of NW in Figure 3b where the arrow indicates the growth direction). First, a stacking fault (SF) nucleates and propagates in the [112] orientation indicative of a stacking fault on a $(1\bar{1}1)$ growth surface (plane F_1 in Figure 4a) while the NW continues to grow in the [111] orientation. During layer-by-layer growth, nucleation at the triple-phase interface is pinned at the intersection of the SF with the top liquid-NW interface. As a result, access to the low energy {111} facet is prohibited, thereby preventing nucleation of any additional defects until the SF is terminated at the opposite side of the NW. Such a SF requires a NW segment length of $d/\tan(19.5°)$ before it terminates at the other surface of the NW, where d is the NW diameter and 19.5° is the angle between the [112] and [111] orientations, and is ∼85 nm for $d = 30$ nm, which is in agreement with experiment (Figure 3b). Once the SF terminates on the opposite side of the NW, access to the low energy {111} facet is again permitted as nucleation of the next atomic layer occurs.

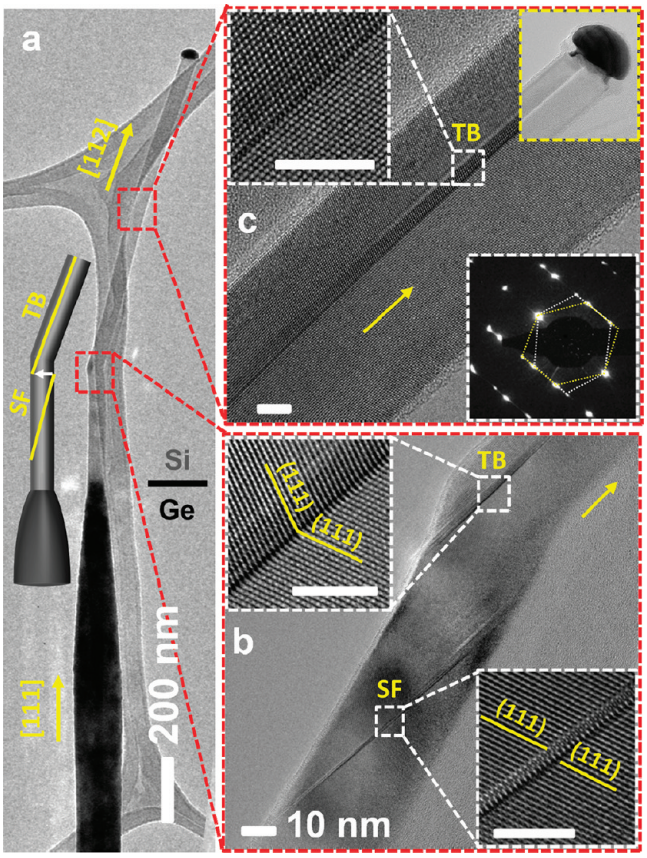

Figure 3. (a) TEM image (right side) and cartoon (left side) of a kinked Ge (dark)−Si (bright) axial NW heterostructure grown by the method of Figure 2 at a SiH_4 partial pressure of ∼1.4 Torr (growth rate was ∼8.3 nm/s). (b) HRTEM image showing nucleation of an intrinsic stacking fault (SF) followed by a Σ3 (111) coherent TB from the same NW facet. Both SF and TB nucleate at $(1\bar{1}1)$ facets and propagate along the [112] direction (see Figure 4 and text). A stacking fault pins the nucleation of each new atomic layer during VLS growth as the fault propagates across the NW such that there is only one fault per NW segment. When the SF terminates at the opposite edge of the NW, a TB immediately nucleates (see Supporting Information Figure S2) from the same $(1\bar{1}1)$ facet side and leads to a kink in NW growth orientation with a kink angle equal to the angle between [111] and [112] orientations (19.5°). Insets show HRTEM images of the SF and TB. Scale bars are 5 nm. (c) Once formed, the TB pins the nucleation for each new atomic layer at the triple-phase interface and continues to propagate during NW growth allowing no further access to the low energy {111} facets and thus no additional fault nucleation. Insets show HRTEM of the TB (upper left), diffraction pattern of twined region (lower right) and TB extending to the Au growth seed (upper right). Scale bars in insets are 5 nm. Yellow arrows in (b) and (c) indicate a [112] NW growth orientation after NW kinking.

From Figure 3b, we observe that a twin boundary (TB) is immediately nucleated at the same low energy $(1\bar{1}1)$ facet at which the preceding stacking fault nucleated, where adatom stacking in two consecutive fault positions leads to TB formation. HRTEM confirms that this process occurs within one atomic layer of the termination of the SF and nucleation switching back to the low energy $(1\bar{1}1)$ facet (Supporting Information Figure S2 shows another HRTEM image at same area of Figure 3b). Once formed, the ledge nucleation occurs at the TB/{110} facet interface and propagates on the two {111} growth surfaces

dx.doi.org/10.1021/nl202126q |*Nano Lett.* 2011, 11, 4200–4206

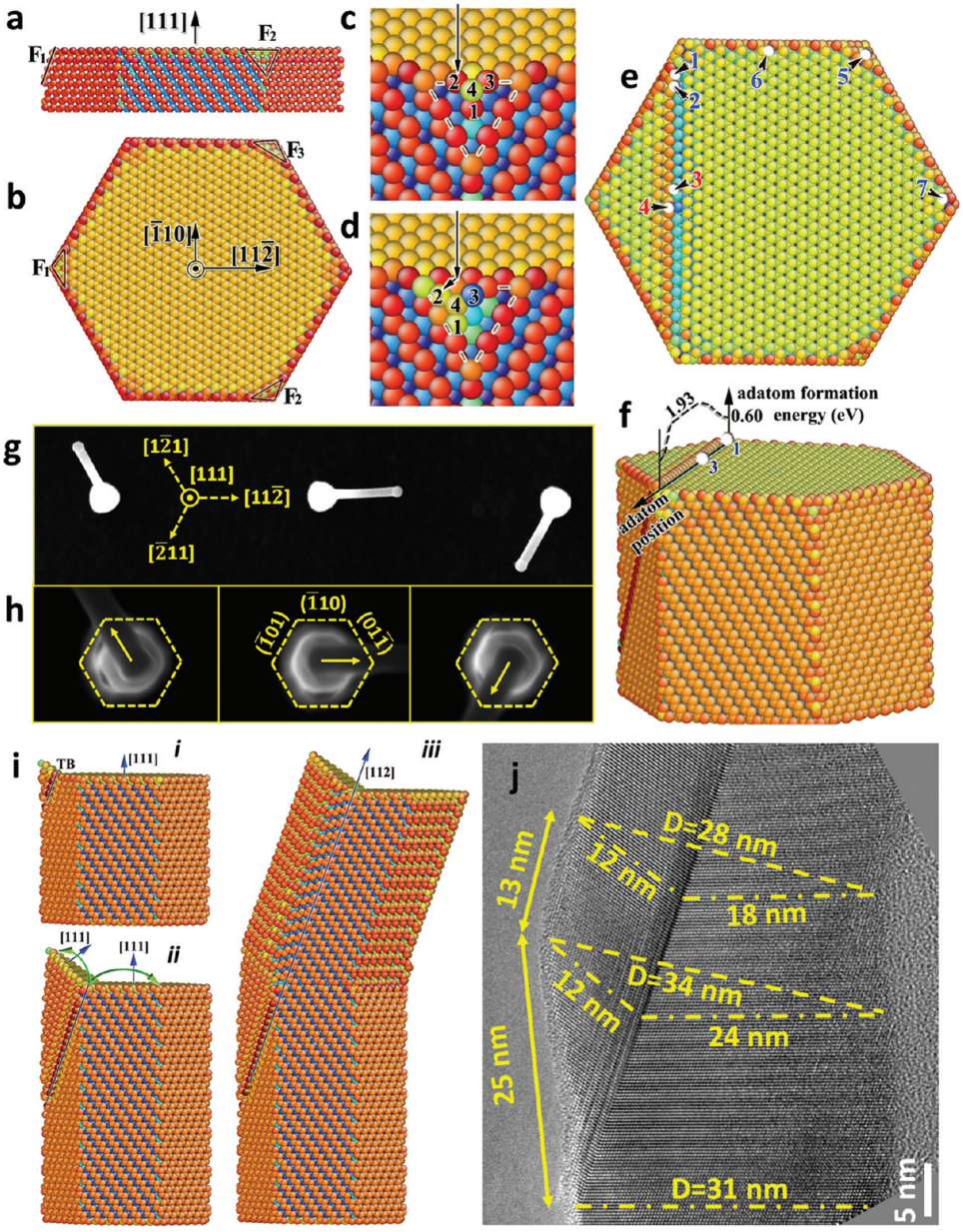

Figure 4. (a,b) Side and top view of a [111] oriented Si NW showing 6 {110} facets with three {111} inclined triangular facets at their intersections. Nucleation at three of these facets, $(1\bar{1}1)$ labeled as F_1, $(11\bar{1})$ as F_2, and $(\bar{1}11)$ as F_3, results in elongation along the NW growth direction, that is, away from the Ge NW base. (c,d) Side view taken from MD simulations showing nucleation on the (111) F_1 facet in proper (c) or faulted (d) positions. The black arrows are inserted to guide the eye for a 4 atom cluster shifting to the faulted position. (e,f) Top (cross-section) and perspective side view of a NW with a stacking fault on the $(1\bar{1}1)$ as used for MD simulations of nucleation energy barriers at points labeled 1−7 in (e), which are 0.6, 1.4, 1.9, 1.93, 1.85, 1.93, and 1.93 eV, respectively. These energies are expected to be lowered in the presence of a liquid growth seed atop the NW. The nucleation energy is lowest at the {110}/SF interface (i.e., SF/triple-phase interface during NW growth). Thus nucleation is pinned at the SF/triple-phase interface and we can only obtain one fault per NW segment, as observed experimentally in Figure 3b. (g,h) High-contrast (g) and low-contrast magnified top view (h) of Ge−Si heterostructure NW growth from lithographically patterned Au dots showing the observed three possible kink directions (projected onto the top (111) plane) in agreement with MD simulations. The dashed arrows in (g) are in-plane projections of [112] Si segment growth orientation. The dashed cylindrical lines in (h) surround the Ge NW {110} facets and the arrow marks the Si NW (smaller diameter and darker contrast) growth direction. Nucleation of the Si segment appears clearly to emerge at two {110} facet interfaces (dashed hexagons in h) corresponding to F_1, F_2, or F_3 in (b). (i) Side-view cartoon showing the progress of the TB from initial formation stage to the formation of the kink in the NW as growth changes from the [111] to the [112] direction. The color scheme in all panels of MD simulation is to provide a perspective of different atomic layers in 3D. (j) HRTEM image of the corresponding observed TB region showing the increase in NW diameter leading to the increased liquid Au line tension and change in growth direction.

(Figure 3b,c) and remains there throughout the growth process. This condition is referred to as the pinning of the nucleation at one point on the triple-phase circumference. The NW diameter consequently increases (see Figure 4j: another HRTEM image at the kink in Figure 3b) until the increasing line tension of the stretched liquid Au surface at the triple-phase interface forces the NW growth direction to switch to the [112] orientation, resulting in a 19.5° kink with respect to the initial [111] growth axis.

dx.doi.org/10.1021/nl202126q |*Nano Lett.* 2011, 11, 4200–4206

Continuum modeling for other cases of NW growth has also noted that perturbations in the line tension of the growth seed may change the NW growth direction.[26]

Ledge nucleation during layer-by-layer growth remains pinned at the TB, preventing access to the low energy {111} facets, and the TB propagation continues to the NW tip (top right inset of Figure 3c). Additional extrinsic SFs near the Ge−Si interface that terminate within few monolayers have also been observed (see Supporting Information Figure S3), but are less common in our NWs. We also note that the presence of SF prior to TB formation is not anticipated to be a necessary condition for a TB stacking sequence to form, but this SF followed by a TB sequence has been observed in four NWs examined in detail with HRTEM for the present growth conditions with a similar structural behavior to the NW described in detail in this manuscript displayed in each case. Also, several tens of NWs that were characterized over the course of two years by TEM and displayed 19.5° kinking have all shown TB in their Si segment when oriented properly into a [110] zone axis in TEM. The relative prevalence of this kinked structure with NW diameter is indicated by the pie charts in Figure 2. We hypothesize that once a particular facet is selected through the formation of a stacking fault, the resulting slight twist in the NW, caused by the additional (111) plane on one side of the fault (left side of the NW in Figure 3b) with respect to the other, may cause the second stacking fault to occur on the same facet (both faults nucleated at the left side of Figure 3b). The possibility of microscopic asymmetries in the facet length at the cross-section of the {110} facets cannot be ruled out; such asymmetries, however, have not been observed in the NWs we examined by SEM as shown in Figure 4h and Supporting Information Figure S5. These striking ex-situ observations of defect nucleation during NW growth establish new features of the VLS mechanism for layer-by-layer NW growth and are further supported by our MD simulations. We note that in situ experiments that discussed pressure induced kinking in Si NWs[9] did not have enough resolution or control over NW orientation during the measurements to resolve such fault and kinking behavior on an atomic scale. We also note that ⟨111⟩ to ⟨111⟩ kinking is frequently observed (Figure 2) and under certain growth conditions, the kink frequency can be pressure controlled.[27]

Wulff constructions for a [111] oriented NW resulted in a hexagonally shaped NW with six {110} type facets parallel to the growth direction. While several reports have inferred {211} type facets for [111] oriented Si and Ge NWs,[10,28] the presence of {110} facets for our growth conditions is demonstrated here by our combined electron microscopy and crystallographic analysis (see also Supporting Information Figures S6 and S7).[29] As shown in Figure 4a,b, three inclined triangular {111} facets occur at the liquid-NW interfaces intersecting the {110} sidewall facets. MD simulations[30,31] (See Supporting Information and Figure S4) have shown that atomic nucleation of succeeding layers in NW growth is energetically preferred at these triangular {111} facets marked F_1, F_2, and F_3 in Figure 4b. Ledge nucleation is thus expected to occur at these inclined {111} facets and propagate on the cross-sectional (111) surface at the liquid−solid interface as each additional atomic layer of NW growth is completed. Such growth behavior from small facets followed by ledge propagation or dissolution at the liquid−solid interface has also been observed using in situ experiments for wurtzite Al_2O_3 NWs,[23] Ge NWs,[32] and Si, Ge, and GaAs NWs.[33] Orienting NWs into a proper zone axis in these in situ studies is tedious and thus classification of the inclined plane at which NW nucleation occurs is nontrivial (added to this are the complexities of the roughening of low-energy facets during growth). These studies are generally at lower growth pressures and infer nucleation on {110} type planes.[31] Since SF and TB defects do not form on {110} planes, nucleation on {110} facets would not appear to apply for our experimental conditions. In our MD simulations, we find that a four-atom cluster growing at the inclined {111} facet not only satisfies minimum energy requirements for nucleation of a stable cluster but is also necessary to maintain the same NW diameter and prevent rapid tapering if nucleation is only to proceed at the plane of the liquid−solid interface. Figure 4c,d shows two possible continuing growth structures: (c) a perfect structure and (d) a faulted structure for the four-atom cluster. MD calculations also showed that the minimum energy for the faulted structure involves a faulted dimer (see also Supporting Information Figure S4).

Ledge propagation then occurs from these {111} facets. By considering different possible nucleation sites for each new layer after SF nucleation, our MD simulations show that cluster nucleation is energetically favorable by ∼2× (see Figure 4f) at the triple-phase interface with the SF (Figure 4e,f). This preference is precisely what imposes the condition of a single defect per NW segment length, as seen in experiment (see Figure 3b). For this condition, the nucleation site moves along the circumference of the NW as layer-by-layer deposition proceeds and the SF moves from the left facet to the right facet of the NW.

To support our hypothesis that the NW nucleation occurs at the inclined {111} facets at the interface between two {110} sidewall facets, we performed Ge−Si heterostructure NW growth from lithographically patterned Au dots on (111) Ge surfaces and observed kinking to typically occur in the three well-defined ⟨112⟩ orientations as projected in the top-view SEM image of Figure 4g. We note that lithographically patterned Au dots are used to exploit the known crystallographic orientation of the Ge(111) substrate that is defined through the initial epitaxial Ge NW growth. Thus we have a reference to determine the kink direction crystallographically for different viewing angles and kink orientations. Low-contrast SEM images have revealed that the kink in the Si segment originates at the interface between two sidewall {110} facets, as labeled in Figure 4h, which is in agreement with our MD simulation results of nucleation at one of the three {111} facets, labeled F_1, F_2, F_3 in Figure 4b. Here, the {110} facet assignment is further supported by the observation of Figure 4h. Since we have determined by TEM that the kinked Si NW grows in the [112] orientation (Figure 3c), and since the direction of the Si NW growth is at 30° angle from the flat sidewall facet in Figure 4h, the sidewall facets are therefore of {110} type facets. Otherwise, the kinked Si NW segment would have to grow and point out from the flat facets if they were {112} type facets, which is contrary to our observations. This analysis assumes the same facets in the Ge and Si segments of the NW, which is consistent with the absence of planar faults perpendicular to the growth orientation of these NWs known to cause rotation. This is further supported by a perfect continuum of lattice structure from the Ge segment of the NW to the Si segment of the NW while both segments remain properly oriented into a ⟨110⟩ viewing direction (Supporting Information Figure S3). As further support for the three kinking directions originating from the interface between two {110} facets,

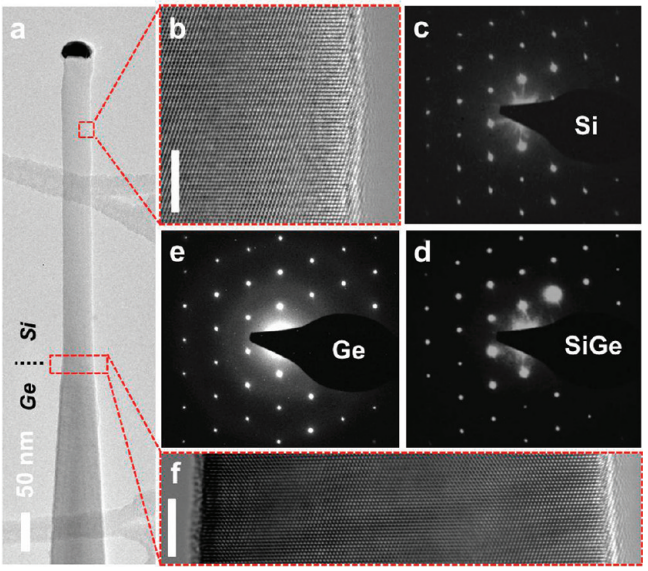

Figure 5. (a) A Si−Ge axial NW heterostructure grown at reduced supersaturations with a SiH_4 partial pressure of ~0.84 Torr (growth rate ~3.75 nm/s). (b) A zoom-in HRTEM image of the Si segment of the NW at a ⟨110⟩ zone axis showing lattice fringes of a single crystal Si segment with [111] growth orientation. (c,d) SAD patterns obtained from the Si, SiGe transition, and the Ge regions demonstrating single crystal structure. (f) HRTEM of the Ge to Si transition region. Scale bars in (b,f) are 5 nm.

Supporting Information Figure S5 shows two separate larger fields of view with systematic kinking of the Si segments from our ordered growth experiments at lithographically defined locations, along with another set of SEM images showing the Si NW segment kink relative to the sidewall faceting. We also note that the twin-boundary line propagating throughout the length of the Si NW segment is observable by SEM as the sample is tilted while maintaining a [110] viewing perspective (Supporting Information Figure S5). Further, larger diameter NWs can show the faceted structure more clearly. In Figure S6, one can see a stacking fault in the Si segment of the NW necessitating that the viewing orientation is a ⟨110⟩ orientation. Since the observed facet in the Ge part of the NW is perpendicular to our viewing orientation, this facet has to be {110} type.

While we find in our experiments a single TB running down the entire Si segment length in support of a single nucleation site at the triple-line interface, there are other reports that found multiple TBs along the length of ⟨112⟩ oriented Si NWs.[8] Such multiple TBs were observed at higher SiH_4 partial pressures than we use here (ref 8 cites 2 Torr for the SiH_4 partial pressure) and therefore at higher supersaturations and growth rates. Prior to kinking into a ⟨112⟩ orientation, the inclined $(1\bar{1}1)$ planes still exist at the NW surface. Ledge nucleation is still thermodynamically expected to happen at the TB/triple-line interface, but as the ledge propagates toward these $(1\bar{1}1)$ facets, Si adatom clusters may deposit at faulty locations at these facets leading to another TB formation. This process can happen multiple times as long as the NW is still growing in the [111] orientation with $(1\bar{1}1)$ facets. As the NW changes to form the kink due to line-tension distortion and resumes growth along a ⟨112⟩ orientation, the NW becomes bounded by a flat $(1\bar{1}1)$ facet and no additional TBs can be formed. Ledge nucleation can happen at any of the TB/triple-line interfaces and these TBs nucleated at the [111] segment of the NW will thus continue down the entire length of the newly formed ⟨211⟩ Si NW segment. We note that the streaks in Figure 3c, just above the TB, are due to local strain and small volume at the edge of the NW but display no additional SFs or TBs.

The nucleation efficiency of the Si segments in the axial Ge−Si heterostructure NWs is increased for growth at high Si supersaturations, however higher supersaturations lead to more kinking. As the NW diameter increases, the facets F_1, F_2, and F_3 of Figure 3b become larger and therefore the stability of a faulted cluster on these facets decrease enabling a self-correction mechanism. As such, larger diameter NWs are expected to have less faults and more straight NWs, which is consistent with experiment as shown in the statistical pie charts of Figure 2. By reducing the SiH_4 partial pressure from 1.4 Torr (Figure 3a) to ~0.84 Torr (Figure 5), we find that the reduced growth rate from 8.3 to 3.75 nm/s results in single crystalline Ge−Si segments without stacking faults or twin boundaries with well-resolved lattice fringes as shown in Figure 5. The partial pressure reduction resulted in a 2× increase in the percentage of straight wires with no noticeable defects, as shown in Figure 5. This reduction is consistent with a kinetic origin of the stacking defects and demonstrates the importance of growth kinetics for structural and morphological control in crystal growth at the nanoscale.

The precise control of growth conditions for Ge−Si axial NW heterostructures is shown to allow 100% composition modulation by the VLS method, providing NWs with segment lengths suitable for exploring novel heterostructure architectures. Through such control of the growth kinetics we provide a comprehensive understanding of the VLS growth mechanism through microscopic observation and atomistic modeling of the nucleation and propagation of stacking defects throughout single nanowires. These defects are found to provide a fingerprint of the layer-by-layer growth process in heterostructured NWs, and provide direct evidence for nucleation of layer-by-layer growth from (111) facets, and reveal how the 19.5° kinking in semiconductor NWs observed at higher Si growth rates results from TB formation. As the TB propagates into the NW it increases locally the NW diameter and therefore distorts the liquid growth seed, increasing the line tension that is restored by the change from a ⟨111⟩ to ⟨211⟩ growth direction. The occurrence of such stacking defects is shown to be reduced by decreasing the growth rate, consistent with a kinetic origin. Such understanding may inspire additional studies on defect control in Ge/Si and other NW material systems.

■ ASSOCIATED CONTENT

Supporting Information. Additional details on the growth, microscopy, and molecular dynamics simulations are discussed with EDS line scans across the interface of different diameter Ge−Si NWs, HRTEM images near the interface, supporting SEM images as well as different perspective atomic ordering obtained from MD simulations for the cases of crystalline and defective cluster nucleation. This material is available free of charge via the Internet at http://pubs.acs.org.

■ AUTHOR INFORMATION

Corresponding Author
*E-mail: shadi@lanl.gov.

■ ACKNOWLEDGMENT

This research was funded in part by the Laboratory Directed Research and Development Program at Los Alamos National Laboratory. The work was performed, in part, at the Center for Integrated Nanotechnologies, a U.S. Department of Energy, Office of Basic Energy Sciences user facility at Los Alamos National Laboratory (Contract DE-AC52-06NA25396) and Sandia National Laboratories (Contract DE-AC04-94AL85000). S.A.D. would like to acknowledge Xiao Hua Liu for providing feedback on the manuscript.

■ REFERENCES

(1) Chau, R.; Datta, S.; Doczy, M.; Doyle, B.; Jen, B.; Karvalieros, J.; Majumdar, A.; Metz, M.; Radosavljevic, M. Benchmarking Nanotechnology for High-Performance and Low-Power Logic Transistor Applications. *IEEE Trans. Elecron Devices* **2005**, *4*, 153.

(2) Gudiksen, M. S.; Lauhon, L. J.; Wang, J.; Smith, D. C.; Lieber, C. M. Growth of Nanowire Superlattice Structures for Nanoscale Photonics and Electronics. *Nature* **2002**, *415*, 617.

(3) Björk, M. T.; Ohlsson, B. J.; Sass, T.; Persson, A. I.; Thelander, C.; Magnusson, M. H.; Deppert, K.; Wallenberg, L. R.; Samuelson, L. One-dimensional Steeplechase for Electrons Realized. *Nano Lett.* **2002**, *2*, 87.

(4) Algra, R. E.; Verheijen, M. A.; Borgström, M. T.; Feiner, L.-F.; Immink, G.; van Enckevort, J. P.; Vlieg, E.; Bakkers, E. P. A. M. Twinning Superlattices in Indium Phosphide Nanowires. *Nature* **2008**, *456*, 369.

(5) Caroff, P.; Dick, K. A.; Johansson, J.; Messing, M. E.; Deppert, K.; Samuelson, L. Controlled Polytypic and Twin-Plane Superlattices in III-V Nanowires. *Nat. Nanotechnol.* **2009**, *4*, 50.

(6) Dayeh, S. A.; Susac, D.; Kavanagh, K. L.; Yu, E. T.; Wang, D. Structural and Electrical Properties of Zincblende and Wurtzite InAs Nanowires. *Adv. Funct. Mater.* **2009**, *19*, 2102.

(7) Davidson, F. M.; Lee, D. C.; Fanfair, D. D.; Korgel, B. A. Lamellar Twinning in Semiconductor Nanowires. *J. Phys. Chem.* **2007**, *111*, 2929 Si NWs in this report were grown by supercritical fluid−liquid−solid growth.

(8) Lopez, F. J.; Hemesath, E. R.; Lauhon, L. J. Ordered Stacking Fault Arrays in Silicon Nanowires. *Nano Lett.* **2009**, *9*, 2774.

(9) Madras, P.; Dailey, E.; Drucker, J. Kinetically Induced Kinking of Vapor−Liquid−Solid Grown Epitaxial Si Nanowires. *Nano Lett.* **2009**, *9*, 3826.

(10) Hyun, Y.-J.; Lugstein, A.; Steinmair, M.; Bertagnolli, E.; Pongratz, P. Orientation Specific Synthesis of Kinked Silicon Nanowires Grown by the Vapor-Liquid-Solid Mechansim. *Nanotechnology* **2009**, *20*, 125606.

(11) Meyerson, B. S.; Jasinski, J. M. Silane Pyrolysis Rates for the Modeling of Chemical Vapor Deposition. *J. App. Phys.* **1987**, *61*, 785.

(12) Smirnov, V. N. Germane Decomposition: Kinetic and Thermochemical Data. *Kinet. Catal.* **2007**, *48*, 1608.

(13) Wu, Y.; Fan, R.; Yang, P. Block-by-Block Growth of Single-Crystalline Si/SiGe Superlattice Nanowires. *Nano Lett.* **2002**, *2*, 83.

(14) Clark, T. E.; Nimmatoori, P.; Lew, K. K.; Pen, L; Redwing, J. M.; Dickey, E. C. Diameter Dependent Growth Rate and Interfacial Abruptness in Vapor−Liquid−Solid $Si/Si_{1-x}Ge_x$ Heterostructure Nanowires. *Nano Lett.* **2008**, *8*, 1246.

(15) Wen, C. Y.; et al. Formation of Compositionally Abrupt Axial Heterojunctions in Silicon-Germanium Nanowires. *Science* **2009**, *326*, 1247.

(16) Picraux, S. T.; Dayeh, S. A.; Manandhar, P.; Perea, D. E.; Choi, S. G. Silicon and Germanium Nanowires: Growth, Properties, and Integration. *J. Metals* **2010**, *62*, 35.

(17) Dick, K. A.; et al. The Morphology of Axial and Branched Nanowire Heterostructures. *Nano Lett.* **2007**, *7*, 1817.

(18) Paladugu, M.; et al. Novel Growth Phenomena Observed in Axial InAs/GaAs Nanowire Heterostructures. *Small* **2007**, *7*, 1873.

(19) Dayeh, S. A.; Huang, J. Y.; Gin, A. V.; Picraux, S. T. Advanced core/multi-shell Germanium/Silicon Nanowire Heterostructures: The Au Diffusion Bottleneck. *Appl. Phys. Lett.*, **2011**, *99*, 023102.

(20) Dayeh, S. A.; Dickerson, R.; Picraux, S. T. Bandgap Engineering in Axial Germanium/Silicon Heterostructured Nanowires. *Appl. Phys. Lett.* **2011**, doi: 10.1063/1.3634050.

(21) Dayeh, S. A.; Picraux, S. T. Direct Observation of Nanoscale Size Effects in Ge Semiconductor Nanowire Growth. *Nano Lett.* **2010**, *10*, 4032.

(22) Glas, F.; Harmand, J.-C.; Patriarche, G. Why Does Wurtzite Form in Nanowires of III-V Zinc Blende Semiconductors. *Phys. Rev. Lett.* **2007**, *99*, 146101.

(23) Oh, S. H.; Chisholm, M. F.; Kauffmann, Y.; Kaplan, W. D.; Luo, W.; Rühle, M.; Scheu, C. Oscillatory Mass Transport in Vapor-Liquid-Solid Growth of Sapphire Nanowires. *Science* **2010**, *330*, 489.

(24) Zhang, X.; Lew, K.-K.; Nimmatoori, P.; Redwing, J. M.; Dickey, E. C. Diameter-Dependent Composition of Vapor−Liquid−Solid Grown $Si_{1-x}Ge_x$ Nanowires. *Nano Lett.* **2007**, *7*, 3241.

(25) Lugstein, A.; Steinmair, M.; Hyun, Y. J.; Hauer, G.; Pongratz, P.; Bertagnolli, E. Pressure-Induced Orientation Control of the Growth of Epitaxial Silicon Nanowires. *Nano Lett.* **2008**, *8*, 2310.

(26) Schwarz, K. W.; Tersoff, J. From Droplets to Nanowires: Dynamics of Vapor-Liquid-Solid Growth. *Phys. Rev. Lett.* **2009**, *102*, 206101.

(27) Tian, B.; Xie, P.; Kempa, T. J.; Bell, D. C.; Lieber, C. M. Single Crystalline Kinked Semiconductor Nanowire Superstructures. *Nat. Nanotechnol.* **2009**, *4*, 824.

(28) Goldthrope, I. A.; Marshall, A. F.; McIntyre, P. C. Inhibiting Strain-Induced Surface Roughening: Dislocation-Free Ge/Si and Ge/SiGe Core−Shell Nanowires. *Nano Lett.* **2009**, *9*, 3715.

(29) {112} type facets are usually found to be non-stable and form {111}, {113}, and {100} facets (see, for example,Verheijen; et al. *Nano Lett.* **2007**, *7*, 3051. If one assumes {111} and {113} facets, three ⟨112⟩ kinking directions would be possible if TB nucleation occurs at the {111} facets, and three ⟨110⟩ kinking directions would be possible with TB nucleation occurring at the {113} facets as indicated schematically in Supporting Information Figure S7.

(30) Wang, J.; Huang, H.; Kesapragada, S. V.; Gall, D. Growth of Y-shaped Nanorods through Physical Vapor Deposition. *Nano Lett.* **2005**, *5*, 2505.

(31) Wang, J.; Huang, H.; Cale, T. S. Diffusion Barriers on Cu Surfaces and near Steps. *Modell. Simul. Mater. Sci. Eng.* **2004**, *12*, 1209.

(32) Gamalski, A. D.; Ducati, C.; Hofman, S. Cyclic Supersaturation and Triple Phase Boundary Dynamics in Germanium Nanowire Growth. *J. Phys. Chem. C* **2011**, *115*, 4413.

(33) Wen., C.-Y.; Tersoff, J.; Hillerich, K.; Reuter, M. C.; Park, J. H.; Kodambaka, S.; Stach, E. A.; Ross, F. M. Periodically Changing Morphology of the Growth Interface in Si, Ge, and GaP Nanowires. *Phys. Rev. Lett.* **2011**, *107*, 025503.

Supporting Materials:

Growth, Defect Formation and Morphology Control of Germanium-Silicon Semiconductor Nanowire Heterostructures

S. A. Dayeh, J. Wang, N. Li, J. Y. Huang, A. V. Gin, and S. T. Picraux

Materials and Methods:

Growth:

Growth of the Ge/Si axial NW heterostructures was carried out in a cold-wall chemical vapor deposition system using GeH_4 (30 % in H_2) and SiH_4 (50 % in H_2) as input precursors and various diameter Au colloids as growth seeds. The growth of Ge NWs was carried out in a two-temperature step process (366 °C nucleation and 276 °C elongation) whereas the growth of the Si segment was carried out at ~ 430 °C – catalyzed at such a low temperature by the Au growth seed with an ~ 1.5 μm long Si segment.

Microscopy:

For transmission electron microscope (TEM) analysis, the as-grown NWs were suspended in an isopropanol solution and deposited on Lacey Carbon TEM grids. A Tecnai F30 TEM was used for structural characterization, HAADF STEM imaging, and EDX analysis.

Molecular dynamics simulations:

The molecular dynamics simulations involve three components: (a) interatomic interactions, (b) setup of simulation cell, and (c) strategy. The interatomic potential of Si adopts empirical potential methods in the form of a Tersoff potential for structural relaxation which is widely

used for group IV semiconductors.[S1] The simulation cell is set up for studying the growth of defects in nanowires and is shown in Fig. 4a-f for a <111>-oriented nanowire. The nanowire has a height of 8.0 nm; its diameter is about 10 nm, whose total volume is limited by the required computational resources. The atoms in the bottom region of the nanowire, three (111) atomic layers, are fixed to mimic an infinite region. The other atoms are free. The initial structure is fully relaxed at a room temperature of 300 K for 40 ps, then further relaxed by using quenching molecular dynamics until the residual force at each atom is less than 5 pN. To understand how stacking faulted structures form, we calculated the formation energies with respect to faulted structures containing an adatom, a dimer, a trimer and a four-atom cluster.[S2, S3] A series of studies were performed using molecular statics method as follows: (1) obtain a relaxed, equilibrium nanowire with 3 triangular {111} facets, (2) determine formation energy of adatom on the triangular {111} facet with respect to perfect crystal sites and faulted crystal sites, (3) determine formation energy of a dimer on the triangular {111} facet with respect to perfect crystal sites and faulted crystal sites, (4) determine formation energy of a trimer on the triangular {111} facet with respect to perfect crystal sites and faulted crystal sites, and (5) determine formation energy of a four-atom cluster on the triangular {111} facet with respect to perfect crystal sites and faulted crystal sites. The results are summarized as follows. An adatom faulted structure (three possible configurations corresponding atom 1, or 2, or 3 in Fig. S4) cannot be stabilized, they instantaneously recover to the perfect crystal sites. A dimer faulted structure can be stabilized. There are six possible configurations (corresponding to the available combinations among the four atoms in Fig. S4). Compared with a perfect crystal (containing a dimer), the energy difference is in the range of 1.98 ~2.37 eV because a dimer has a different formation

energy in the perfect crystal. There are also six possible structures of a trimer. Comparing with perfect crystal (containing a trimer), the formation energy difference is in the range of 4.54 ~4.64 eV. There is only one structure for a four-atom cluster (Fig. S4), the formation energy difference is 6.32 eV. The results show that a stabilized stacking fault structure forms with a dimer when the dimer grows on the faulted crystal sites (F1, F2 or F3 in Fig. S4). Once a stacking fault forms and grows during the nanowire synthesis, we further calculated formation energies of adatoms located at different sites, as shown in Fig S4. The results show the preferred nucleation site is at the {110}/SF interface (i.e. SF/triple-phase interface during NW growth).

S1 J. Tersoff, New Empirical Approach for the Structure and Energy of Covalent Systems, *Phys. Rev.*, B **37**, 6991-7000 (1988).
S2 J. Wang, H. Huang, S. V. Kesapragada, D. Gall, Growth of Y-shaped Nanorods through Physical Vapor Deposition. *Nano Lett.* **5**, 2505-2508 (2005).
S3 J. Wang, H. Huang, T. S. Cale, Diffusion Barriers on Cu Surfaces and near Steps, *Modeling and Simulation in Materials Science and Engineering* **12**, 1209-1225 (2004).

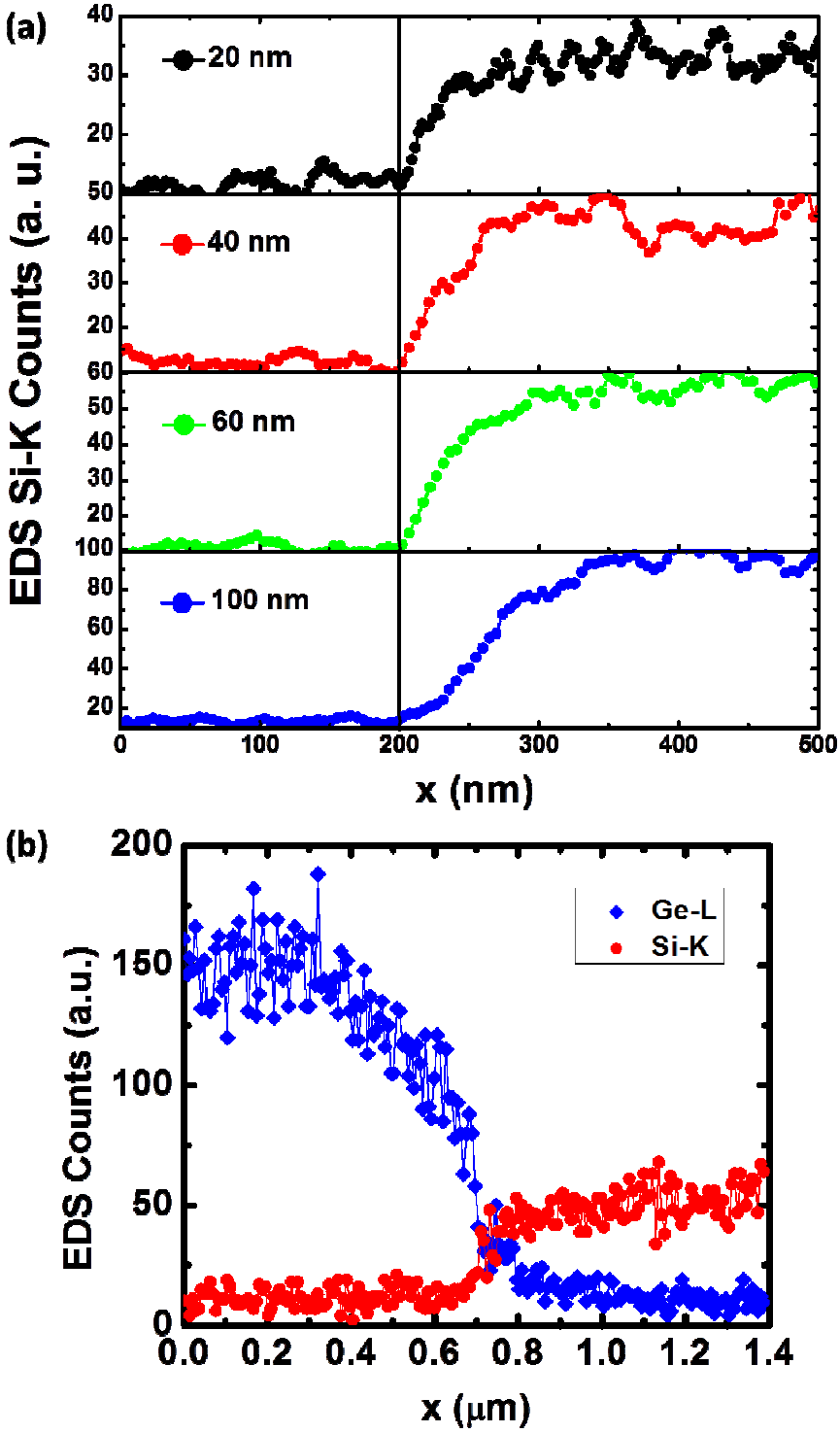

Fig. S1: (a) EDS line scan showing the Si-K line for different diameter NWs. The absolute value of the SiGe transition region (composition change from 10 to 90 %) increases as the NW diameter

increases. Relative to the NW diameter, the SiGe transition region was found to be ~ 0.85 d – 1.4 d for d= 40 nm – 100 nm, and ~ 2d for $d \leq$ 30 nm, where d is the NW diameter. (b) EDS line scan for Si-K and Ge-L lines for a 40 nm diameter NW showing complete suppression of the Ge signal to the noise level. The sloped shape for the Ge signal in the first 0.7 μm is due to the tapered Ge segment (grown during temperature ramp).

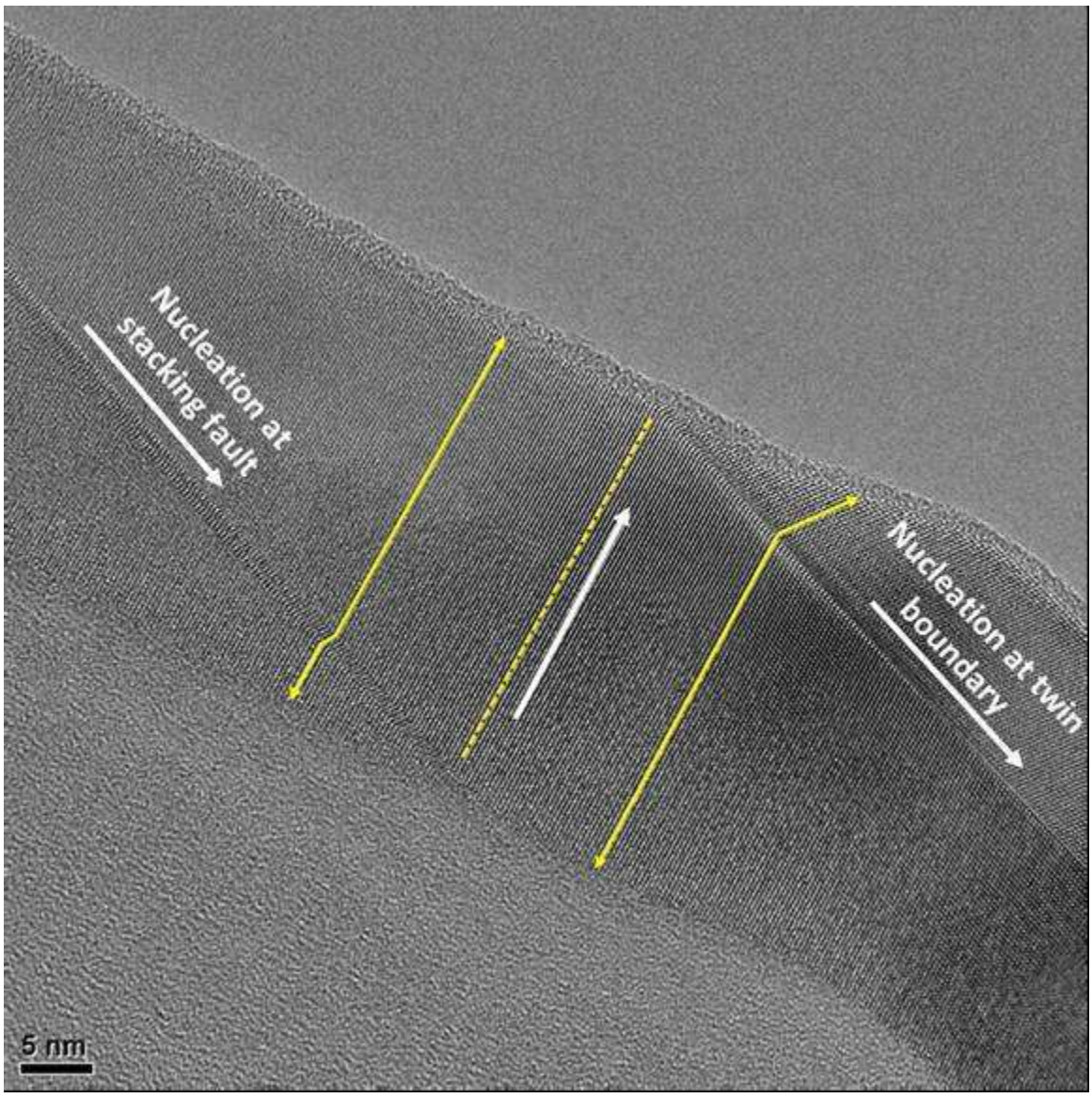

Fig. S2: HRTEM image at the Si NW segment (corresponding to that of Fig. 2) showing termination of the stacking fault at the edge of NW and immediate nucleation of the twin boundary at the low energy {111} facet at the other edge of the NW. The transition happens within one atomic layer (indicated by dashed yellow line and white arrow through the NW cross-section) where the SF terminates and the new layer nucleates in a faulted position at the opposite edge of the NW.

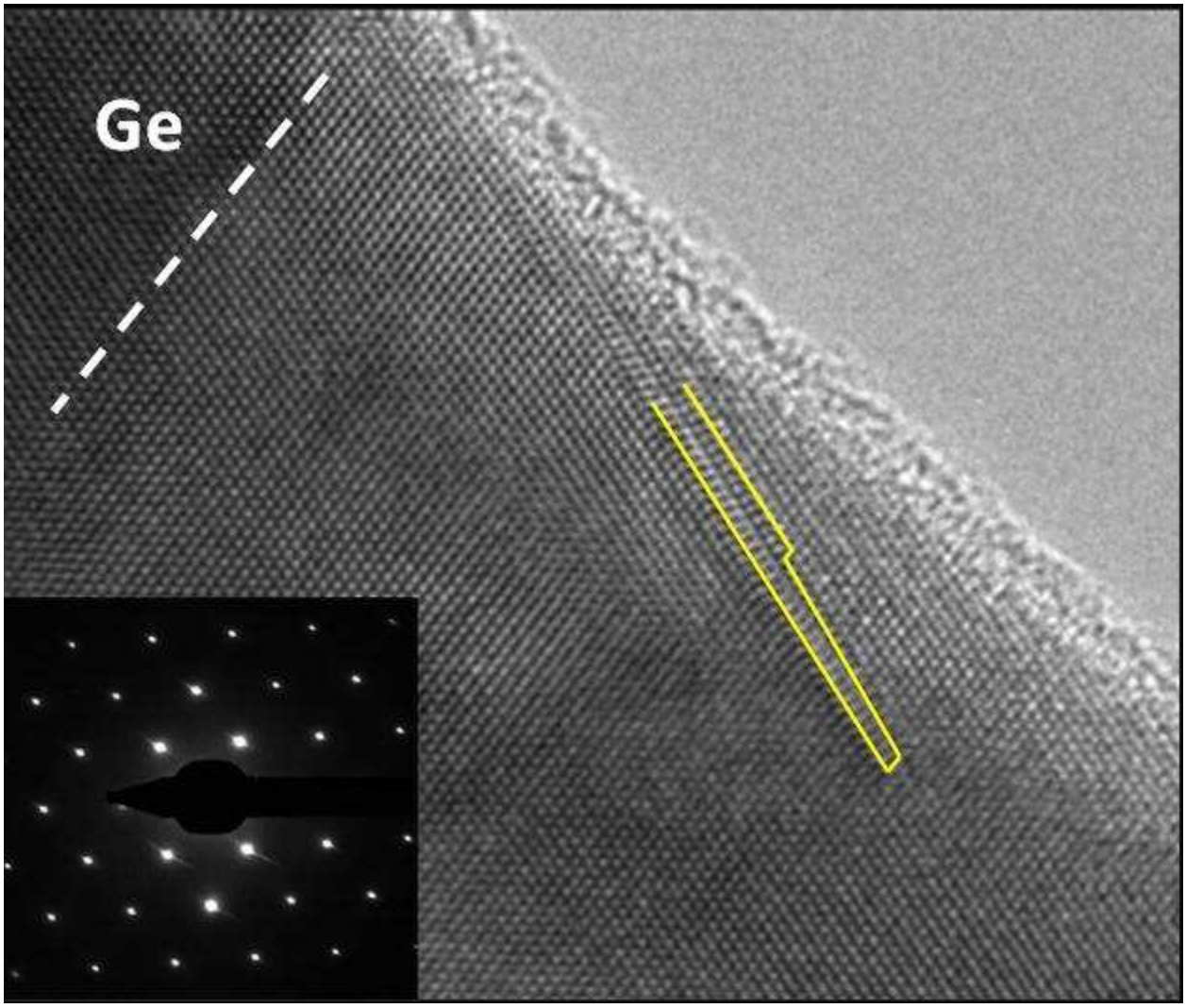

Fig. S3: HRTEM image at the Ge/GeSi interfacial region showing an extrinsic stacking fault which terminates without propagation to the other edge of the NW (Fig. 2B). Inset is an SAD pattern that shows a monocrystalline structure at the interface.

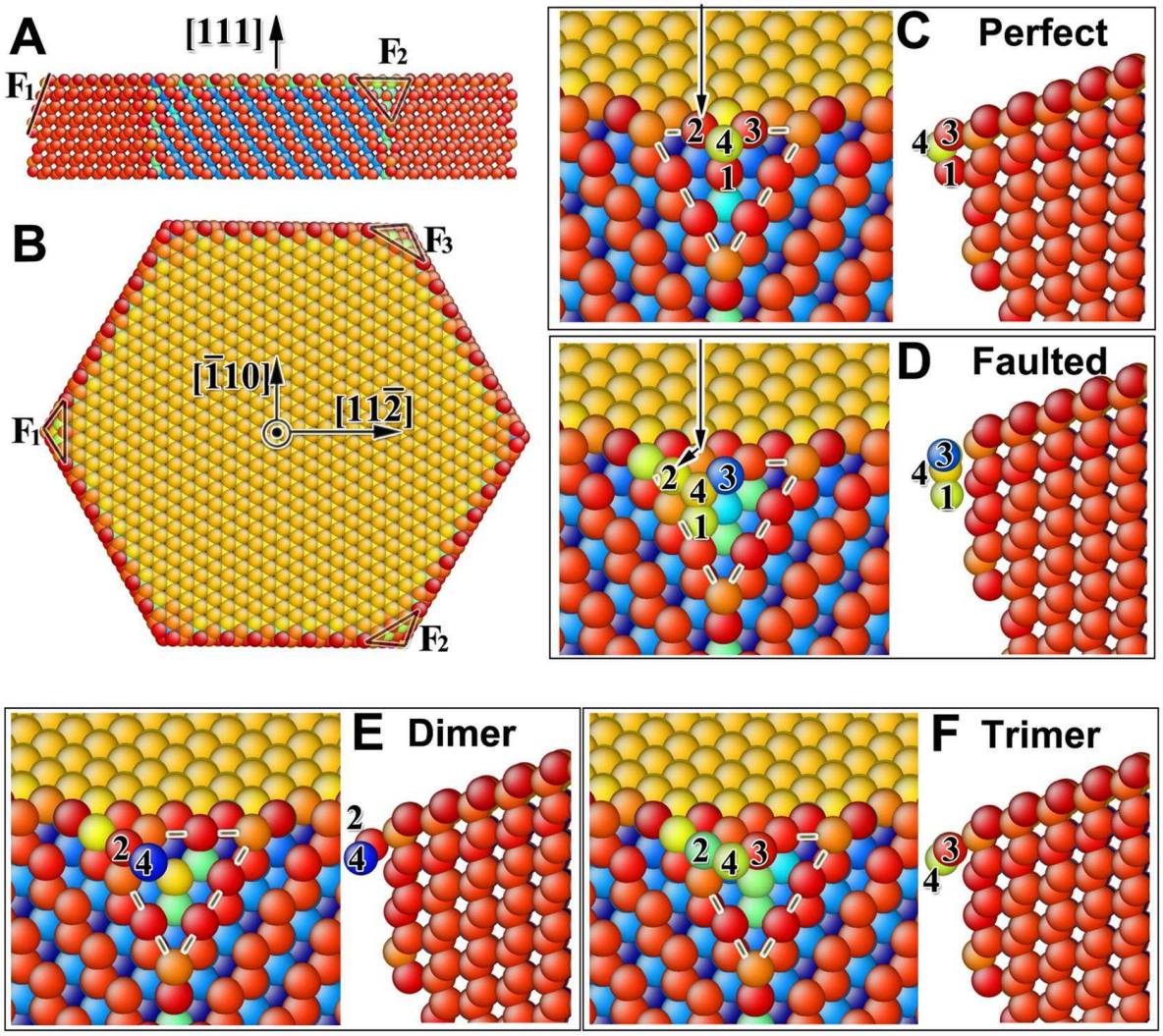

Fig. S4. (**A, B**) Top and side view of a [111] oriented Si NW showing six {110} facets with three {111} triangular facets at their intersection. Nucleation at three of these facets, $(1\bar{1}1)$ labeled as F_1, $(11\bar{1})$ as F_2, and $(\bar{1}11)$ as F_3, can result in NW elongation within 0° – 90° of the NW axis, i.e. away from the Ge NW base. (**C, D**) Side view of graphs showing nucleation of a four-atom cluster at the (111) F_1 facet in (C) perfect crystal sites or (D) faulted crystal sites. The black arrows are inserted to guide the eye for cluster shifting to the faulted position. (**E, F**) Side view-graphs showing nucleation of a dimer and a trimer at the (111) F_1 facet in faulted crystal sites. The numbers (1-4) marked at atoms shows their positions relative to the perfect crystal. The color scheme in all panels of is to provide a perspective of different atomic layers in 3D.

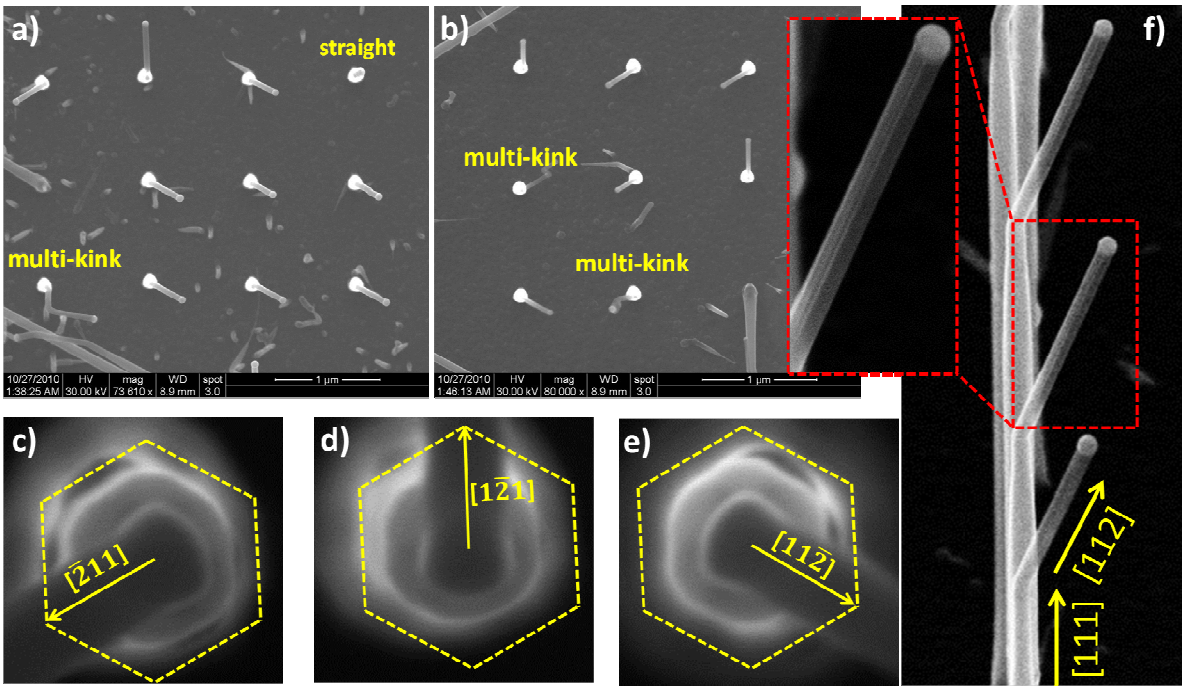

Fig. S5: a,b) Top-view SEM images at 2 separate locations from ordered array growth of Ge-Si NW heterostructures showing 3 predominant kink orientations. c-e) Hexagonal NW shape with six {110} facets are clearly visible in the low-contrast SEM images with nucleation and growth of the Si NW segment from the interface intersection between these {110} planes. The three vectors indicate the projection of the kinked segment on the growth plane (111). f) Oblique angle view of portion of the NW array showing 3 NWs with a twin boundary apparent in the kinked Si NW segment under SEM and can be clearly seen in the magnified image to the left of panel (f).

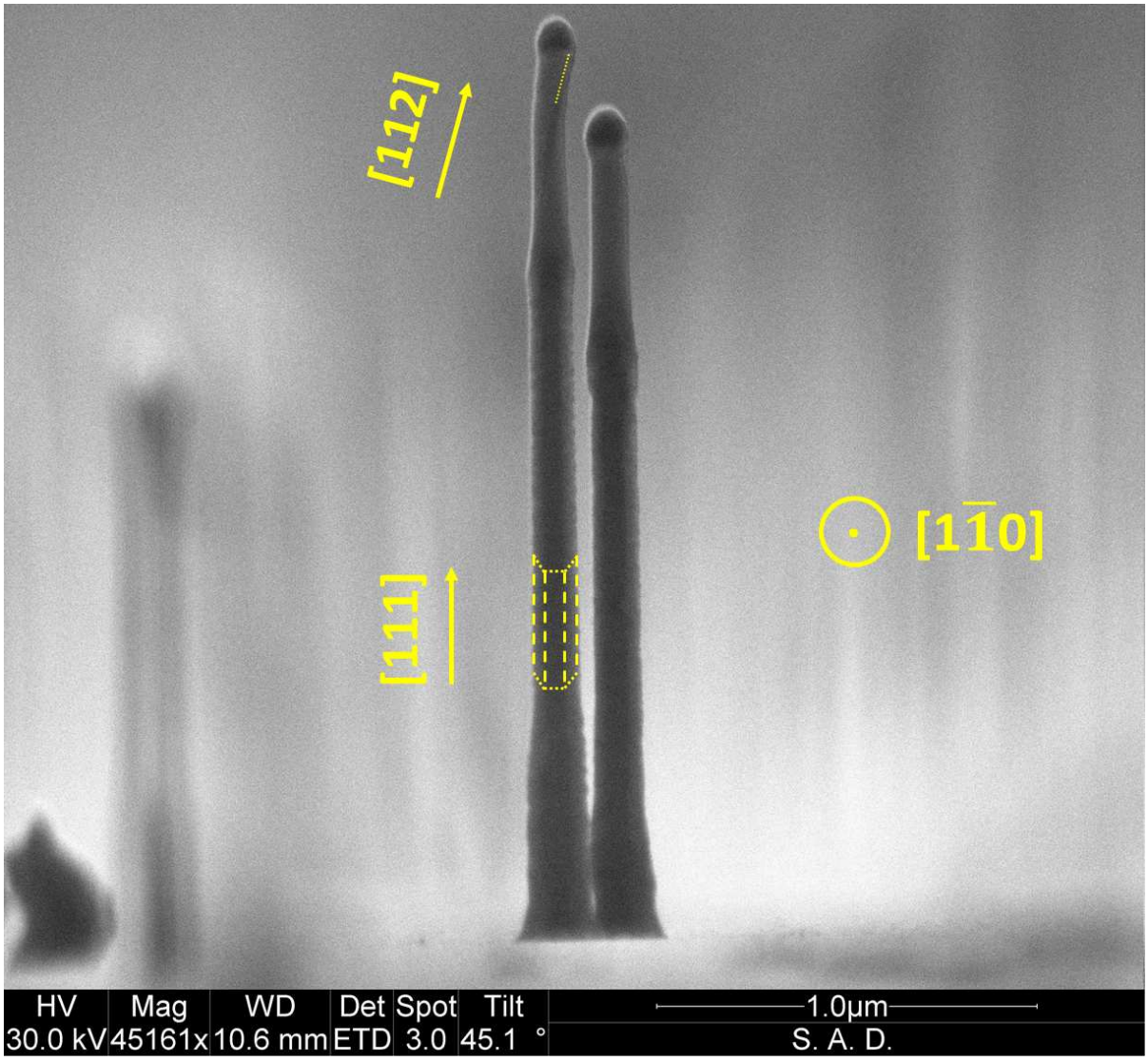

Fig. S6: Cross-sectional SEM image of axial Ge-Si heterostructure NW grown using method 1 of GeH_4 pulsing (see text). One can see in the Si segment of the left NW a stacking fault that propagates at an angle of ~ 20° with respect of the growth axis, part of which is marked with a yellow dotted line close to the Au particle. This establishes that we are viewing the NW from a <110> orientation. At the Ge segment of the NW, we can see a flat facet in the center of the NW perpendicular to our viewing direction. This validates that this NW has {110} type facets.

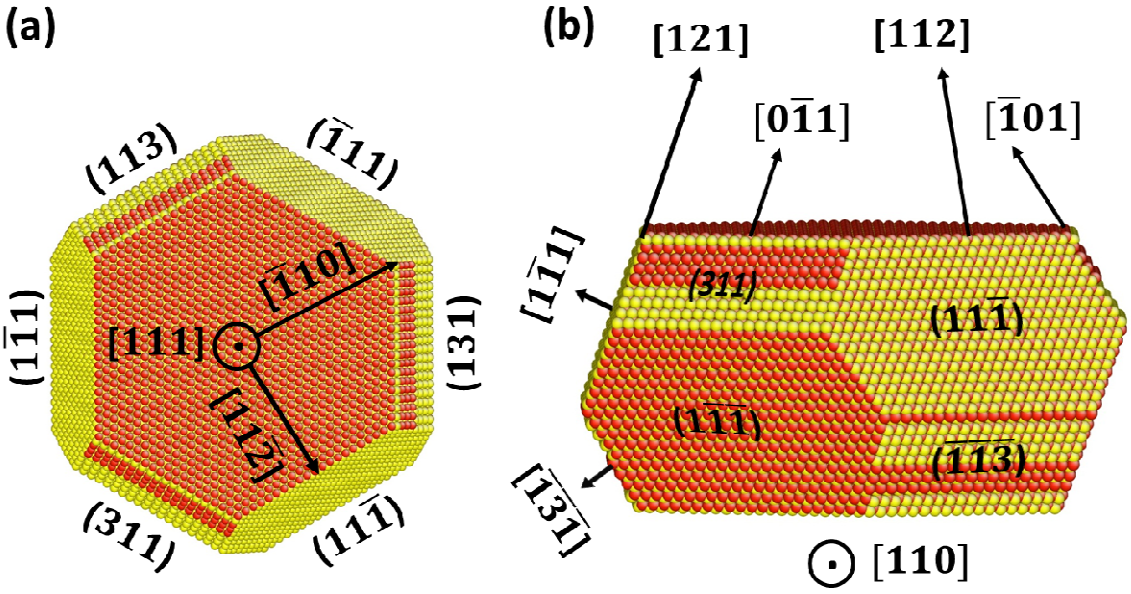

Fig. S7: (a) Top view of a NW model with [111] growth orientation and sidewalls perpendicular to the <112> orientations. This corresponds to a {111} oriented NW with (211) sidewall facets that have decomposed into (111) and (311) facets due to their lower net surface energy. Such structures have been observed by in situ TEM studies of NW growth at lower pressures than used here. (b) Same as in (a) viewed at its side along a [110] direction showing that if TB nucleation occurs at the inclined {111} planes, kinking into three <112> orientations would be possible and that if TB nucleation occurs at inclined {113} planes, kinking would instead occur into the three [110] orientations.